Electronic equivalence of optical negative refraction and retroreflection in the two-dimensional systems with inhomogeneous spin-orbit couplings

Bo Lv and Zhongshui Ma[*]
School of Physics, Peking University, Beijing 100871, China

(Received 17 May 2012; revised manuscript received 29 November 2012; published 9 January 2013)

The negative refracted transmission and retroreflection of electrons in low-electron-density semiconductors, in the presence of spin-orbit coupling, are theoretically predicted. It is shown that negative electronic transport may occur owing to the occurrence of additional states whose wave vectors are antiparallel to their group velocities. We conclude that the transport emerges as negative in nature in the scattering process if the sign of its ray equation is reversed with respect to that of the incidence's. We demonstrate this finding in the hybrid of two-dimensional electron gases with different Rashba spin-orbit couplings. We also show that the fundamental of negative electric transport is promising to focus a divergent electronic beam in a spintronic sandwich structure with flat surfaces.

DOI: 10.1103/PhysRevB.87.045305 PACS number(s): 72.25.Mk, 42.15.Dp, 42.25.Gy, 85.75.Hh

I. INTRODUCTION

The influence of spin-orbit interaction (SOI) on the transport properties has been a subject of considerable investigation for many years.[1–5] Owing to the SOI effect, a spin-degenerate parabolic band is split into two spin-helicity bands. In general, electrons fill in both the bands with two oppositely spin-polarized states. The existence of two spin-polarized states leads to many extraordinary phenomena in spintronic tunneling in hybrids with different SOIs, such as bidirectional refraction[6] and spin optics.[7] Electrons reflected at the interface between two-dimensional electron gases (2DEGs) with a step-like variation of the SOI strength changes the spin orientation via the spin angular impulse exerted on electrons[8] and produces an edge spin current.[9] Recent experiments revealed that all electrons can be restricted in one of the spin-helicity bands in low-density semiconductors with a strong SOI.[10–12] The Fermi energy and Rashba spin splitting can be tuned in spintronic systems,[13] graphene,[14] and 2DEGs in a topological insulator.[15] Theoretically, the spin accumulation for the case of electrons filling in a single spin-helicity band, due to the interference of incident and reflected electron waves, was studied.[16] Corresponding to the variation of the electronic structure from two spin-helicity bands to a single spin-helicity band, the differential-geometric characteristics of the Fermi surface are changed.[17,18] One of the most remarkable characteristics is that the density of states (DOS) is no longer a constant as it would be for a 2DEG, while a one-dimensional (1D) feature emerges. Another characteristic accompanied by topological variation of the Fermi surface is that the relative orientations of the Fermi wave vector and the group velocity of the electronic wave packet can emerge antiparallel to each other.

Recalling a counterintuitive phenomenon relating to the group velocity antiparallel to the wave vector, Veselago[19] predicted the existence of negative refraction in the crystal optics. This phenomenon had been demonstrated in microwave scattering experiments.[20–24] Analyzing these artificially structured materials, with negative refractive indices, consisting of simultaneously double-negative permittivity and permeability material[25,26] or consisting of a periodic arrangement of scatterers in the photonic crystal,[27] it is found that they have common and fundamental characteristics, i.e., the group and phase velocities are in opposite directions.[28] The relative orientation between the group and the phase velocities can be characterized intuitively by the sign of a ray equation,[29,30] which is defined as a scalar product of group and phase velocities. Because the propagation of a wave with a negative sign in the ray equation behaves differently from that of a wave with a positive sign, the change in sign of the ray equation across the interface between two materials has been predicted to exhibit a variety of novel electromagnetic phenomena.[31]

It is of interest to investigate whether or not there exists an electronic analog of optical negative refraction or, more generally, "negative" electronic transport in semiconductors. Here "negative" means that an oblique incidence of electron beam at the interface of two different materials is transmitted and reflected to the same side of the incidence's with regard to the normal at some angles. The transport behavior is determined by the dispersion law of particles. Negative refraction has been predicted in spintronic and graphene systems. By analyzing the special dispersion law derived from a non-Abelian potential, Juzeliūnas *et al.* recently predicted that negative refraction[32] and negative reflection[33] of cold atoms can be achieved in cold atom systems. Cheianov *et al.* predicted the negative refracted character of electronic transmission in a graphene p-n junction.[34] In studies of spin-polarized tunneling Zhang[35] considered a heterostructure consisting of two regions without SOI and with both Rashba[36,37] and Dresselhaus[38] SOI. It was found that one of the propagating modes itself manifests a negative refraction. To date the retroreflection of electrons is still a rare physical phenomenon and has not been discussed. The retroreflection of electrons cannot happen in graphene. Although negative reflection has been predicted for the Andreev[39] reflection in graphene[40] and spintronics[41] systems, electronic negative transport in semiconductors so far has not been studied systematically.

The purpose of this paper is, first, to investigate the electronic conditions that are analogous to those of optical negative refractive behavior and, second, to extend the analysis to "negative" electronic transport in semiconductor heterostructures with inhomogeneous SOI. We show that the group velocity of electrons can be antiparallel to the phase velocity in low-density spintronic systems where the electrons are restricted to one helicity band. The antiparallel nature provides an internal link with the optical effect of negative refraction. Correspondingly, not only negative refraction but also retroreflection of electrons is found in hybrid systems made of semiconductors with different SOIs. We show that the occurrence of negative electronic transport can be justified by the sign reversal of ray equations in the scattering processes. Our conclusion is that the occurrence of negative transport relates to the appearance of negative-oriented states, which is associated with the nontrivial configuration of 1D spin-polarized Fermi surfaces at a low electron density and with a strong SOI. According to our analysis negative electronic transport could not be realized in the previous work with two concentric Fermi disks of oppositely spin-polarized states. We also show that the variation of DOS dimensional characteristics from two to one dimension occurs in the wake of sign reversal in the ray equation. Similarly to these dramatic effects on electronic transport in the Lifshitz transition,[42] such nuances owing to the topological variation of Fermi surfaces would be of interest to the low-dimensional quantum condensed matter systems with a Fermi surface changing. We demonstrate the occurrence of negative refracted transmission in a hybrid of normal 2DEG (N2DEG) and a 2DEG in the presence of Rashba SOI (R2DEG)[36] and retroreflection in a hybrid of R2DEG/N2DEG. With these two systems, the angular dependencies of electronic fluxes of various propagating modes can be treated consistently. The finding in this paper may allow practical realization of electronic focusing in a sandwich structure of an N2DEG/R2DEG/N2DEG heterojunction.

The paper is organized as follows. Section II defines the ray equations for the electronic propagation modes in spintronic systems. The change of the differential-geometric configuration of Fermi surfaces is analyzed accordingly. In Sec. III, we discuss the essential relationship between the sign reversal of ray equations and the occurrence of negative propagation modes in the scattering processes. Section IV generalizes the analysis of negative refracted transmission and retroreflection in R2DEG heterostructures with inhomogeneous SOI. The angular dependencies of negative refraction and reflection fluxes are treated consistently. We analyze the deductions of conduction from the retroreflections. The partial conductances accrued from negative refractions (transmissions) are calculated. In Sec. V observations in physical systems and realization of electronic focusing in a sandwich structure of an N2DEG/R2DEG/N2DEG heterojunction are suggested. Finally, we present the conclusions and discussions in Sec. VI.

II. RAY EQUATIONS FOR ELECTRONIC PROPAGATION MODES

A. Electronic ray equations

Let us first consider an energy spectrum of 2DEG with a dispersion law

$$\varepsilon = A\,(k-a)^2\,, \tag{1}$$

where $k=\sqrt{k_x^2+k_y^2}$ is the absolute value of wave vector $\mathbf{k}$. The energy has an annular minimum $\varepsilon=0$ at $k=a$ and a bulging $\varepsilon=Aa^2$ at $\mathbf{k}=0$. For the incident energy

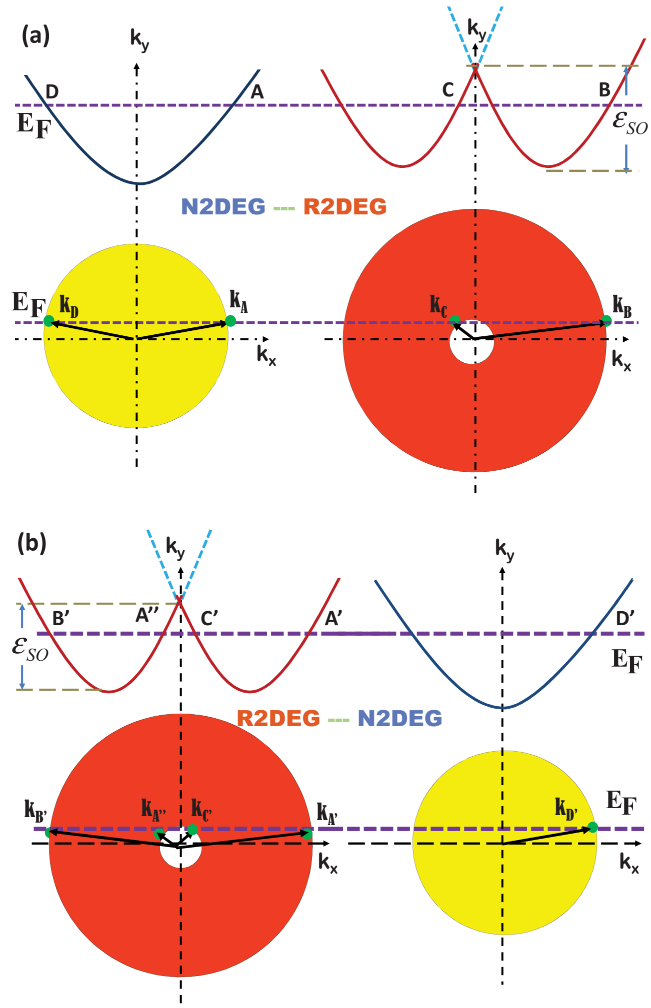

FIG. 1. (Color online) Diagrammatic sketch of band structures and various k positions for incident, reflected, and transmitted electrons in (a) N2DEG/R2DEG and (b) R2DEG/N2DEG. An electron with an energy ϵ intersects the negative branch (red curve).

of electrons lying slightly below the bulging ($\varepsilon < Aa^2$), the equienergy surface demonstrates the geometry of an annular disk, shown by the right (red) circle in Fig. 1(a) and the left (red) circle in Fig. 1(b). The radii of the outer and inner edges are $k_+ = a+\sqrt{\varepsilon/A}$ and $k_- = a-\sqrt{\varepsilon/A}$, respectively. Corresponding to an increase in energy $\delta\varepsilon$, these two radii change, $\delta k_\pm = \pm(1/2\sqrt{A\varepsilon})\delta\varepsilon$; i.e., the outer circle tends to be enlarged while the inner circle tends to be reduced. This equienergy annular disk can be divided into two regimes by a demarcation circle of radius $k=a$, where $\partial\varepsilon/\partial k=0$. The curvature $\partial\varepsilon/\partial k$ alternates the sign across the demarcation circle; i.e.,

$$\frac{\partial\varepsilon}{\partial k}\begin{cases} >0 & \text{if} \quad k_+ \geqslant k > a, \\ <0 & \text{if} \quad a > k \geqslant k_-. \end{cases} \tag{2}$$

The wave vectors ending at the edges of the equienergy surface determine the electronic propagation modes. Thus, if $\varepsilon < Aa^2$, there exist two allowed propagation modes whose wave vectors end at the edges of the outer and the inner circles of the equienergy annular disk, respectively. In the quantum mechanics description, the true direction of electronic transport is determined by the group velocity of electrons, which is defined by the canonical momentum of electrons rather than the momentum. The latter determines the phase velocity of electronic waves. The group velocity is defined by the variance of energy with respect to the momentum $\mathbf{v}_g = \hbar^{-1}\nabla_{\mathbf{k}}\varepsilon$. If ε is the function of k only, it can be written in the form $\mathbf{v}_g = \mathbf{k}(k\hbar)^{-1}\partial\epsilon/\partial k$. Because of the factor $\partial\varepsilon/\partial k$, the group velocity can be in a different direction from the phase velocity, owing to the particular functional dependency of the dispersion law on the momentum. From Eq. (2) the curvatures $\partial\varepsilon/\partial k$ at the two edges of the equienergy annular disk have opposite signs. Thus, the direction of group velocity is parallel to that of the wave vector when $\mathbf{k}$ ends at the outer circle and opposite to the wave vector when $\mathbf{k}$ ends at the inner circle. It follows that

$$\mathbf{k}\cdot\mathbf{v}_g = \begin{cases} 2k_+\sqrt{A\varepsilon}/\hbar & \text{if} \quad \mathbf{k} \text{ on outer circle,} \\ -2k_-\sqrt{A\varepsilon}/\hbar & \text{if} \quad \mathbf{k} \text{ on inner circle.} \end{cases} \tag{3}$$

Because $\mathbf{v}_g\cdot\mathbf{v}_g|_{k_\pm} = 4A\varepsilon/\hbar^2$, we can define the ray vector of the electron beam by scaling the magnitude of group velocity as $\mathbf{s} = \mathbf{v}_g/(2\sqrt{A\varepsilon}/\hbar)$. Equation (3) becomes

$$\mathbf{n}_\pm\cdot\mathbf{s}_\pm = \pm 1, \tag{4}$$

where $\mathbf{n} = \mathbf{k}/k$. These are ray equations for two propagation modes. The sign of $\mathbf{k}\cdot\mathbf{v}_g$ in Eq. (3) is then delineated by the sign of the ray equation. A positive sign in the ray equation corresponds to a positively oriented state, while a negative sign corresponds to a negatively oriented state.

B. The topological structure of Fermi surfaces

The aforementioned dispersion law in Eq. (1) can be realized in 2D electronic systems with SOI. In general, the Hamiltonian can be written in the form

$$H = \mathbf{p}\frac{A}{\hbar^2}\mathbf{p} + \left\{\sigma\cdot\mathbf{p},\frac{B}{\hbar}\right\} + \widehat{e}_z\cdot\left\{\sigma\times\mathbf{p},\frac{C}{\hbar}\right\} + Aa^2, \tag{5}$$

where A is the intrinsic parameter of electrons, B and C are the internal and external parameters, and $a = \sqrt{B^2+C^2}/2A$. In general they are spatially dependent because of the spatial inhomogeneity of the effective mass, the charge density, and the strength of SOI in semiconductor heterostructures. We assume that the spatial variations of these parameters occur only at interfaces and that they are constants in regions away from the interface. In the region away from the interface, the eigenstate can be written in the form $\psi = \xi e^{i\mathbf{k}\cdot\mathbf{x}}$. The Hamiltonian becomes

$$H_k = A\mathbf{k}^2 + B\left[\sigma\cdot\mathbf{k} + \tan\beta\widehat{e}_z\cdot(\sigma\times\mathbf{k})\right] + a^2, \tag{6}$$

where $\beta = \arctan(C/B)$. The eigenenergies $\varepsilon_\pm = A(k\pm a)^2$ and the eigenstates

$$\xi_\pm = (1/\sqrt{2})(\pm e^{-i(\theta_{\mathbf{k}}-\beta)}\ 1)^{\mathcal{T}}$$

are found, where $\mathcal{T}$ represents the transpose, and $\theta_{\mathbf{k}} = \arctan(k_y/k_x)$ is the oblique angle of $\mathbf{k}$. The two spin-splitting bands $\varepsilon_\pm$ cross at the energy bulging.

The DOS is given as

$$D(\varepsilon) = \frac{1}{2\pi A}\left[\Theta(\varepsilon - Aa^2) + \frac{a\sqrt{A}}{\sqrt{\varepsilon}}\Theta(Aa^2-\varepsilon)\right], \tag{7}$$

where $\Theta(x)$ is the Heaviside step function. This DOS reveals the distinct characteristics for the energy above and below the energy bulging $\epsilon = Aa^2$. Equation (7) shows that the DOS has 2D characteristics if $\varepsilon > Aa^2$ but 1D characteristics with van Hove singularity behavior[17] emerge if $\varepsilon < Aa^2$.

The Fermi surfaces then have different geometric structures for $\varepsilon_F > Aa^2$ and $\varepsilon_F < Aa^2$. If the Fermi energy ε_F lies slightly above the energy bulging ($\varepsilon_F > Aa^2$), it intersects two opposed spin-helicity bands. $\varepsilon_F = A(k'_F \pm a)^2$ identifies two concentric Fermi disks of radii $k'_{F,\pm} = \sqrt{\varepsilon_F/A} \mp a$. The Fermi energy is linear in the density of electrons n_e. However, for the case where the Fermi energy lies below the energy bulging ($\varepsilon_F < Aa^2$), it intersects only the band $\varepsilon_F = A(k_F - a)^2$. As a consequence, a chiral material with only state ξ_- is achieved. The Fermi surface is in the form of an annular disk bound by Fermi wave numbers $k_{F,\pm} = a \pm \sqrt{\varepsilon_F/A}$. The Fermi energy is quadratic in the density of electrons, $\varepsilon_F = (\pi\sqrt{A}/a)^2 n_e^2$. Thus, the geometric characteristics of the Fermi surface can be controlled by the electron density and the external actions ($n_e \lesssim a^2/\pi$).

In the case of $\varepsilon_F > Aa^2$ two spin-polarized states have the same ray equation, $\mathbf{n}_F\cdot\mathbf{s}_F = +1$. However, for $\varepsilon_F < Aa^2$ the ray equations of two propagating modes $\mathbf{k}_{F,\pm}$ have opposite signs, $\mathbf{n}_{F,\pm}\cdot\mathbf{s}_{F,\pm} = \pm 1$. According to the analysis in Sec. II A, only positively oriented states exist for $\varepsilon_F > Aa^2$. But both positively oriented states $\mathbf{k}_{F,+}$ and negatively oriented states $\mathbf{k}_{F,-}$ can occur for $\varepsilon_F < Aa^2$. The occurrence of a negatively oriented mode $\mathbf{k}_{F,-}$ implies the interplay of change in the topological structure of the Fermi surface and dimensional variation in the DOS. Topological change of the Fermi surface gives rise to an additional negative-oriented state.

III. NEGATIVE REFRACTED TRANSMISSION AND RETROREFLECTION

To analyze the electronic analog of an optical negative refraction, we first investigate electron tunneling across the interface between two 2DEGs with different spin-splitting constants B and C. We then extend the analysis to the retroreflection of electrons.

A. Negative refracted transmission

We consider a hybrid of two 2DEGs with SOI present only on the right side of the interface. The interface is situated at $x = 0$ as shown in Fig. 1(a). The system is described by Hamiltonian (5) with $B = b\Theta(x)$ and $C = c\Theta(x)$. The Fermi levels on the two sides of the interface align if no bias is applied across the junction. Applying a low voltage across the junction, electrons tunnel through the interface from left to right along the x axis. For an incident electron with energy $\varepsilon < Aa^2$, the dispersion relations for electrons on the two sides are $\varepsilon = Ak^2$ and $\varepsilon = A(k-a)^2$, respectively. The electronic incidence and reflection are in spin-degenerate states, while the transmission is in spin-polarized states ξ_-. There are one reflected mode with $\mathbf{k}$ in the region $x < 0$ and two transmitted modes in the region $x > 0$. The wave vectors of two transmitted modes are $\mathbf{k}_+ = \mathbf{k}_B$ and $\mathbf{k}_- = \mathbf{k}_C$ ($k_\pm = |\mathbf{k}_\pm| = a \pm \sqrt{\varepsilon/A}$) as shown in Fig. 1(a). The group velocities of transmitted electrons for the

$\mathbf{k}_B$ and $\mathbf{k}_C$ modes are

$$\mathbf{v}_g^B = 2\sqrt{\varepsilon/A\hbar^2}\left(\sqrt{1-k_y^2/k_+^2}e_x + k_y/k_+e_y\right) \tag{8}$$

and

$$\mathbf{v}_g^C = 2\sqrt{\varepsilon/A\hbar^2}\left(\sqrt{1-k_y^2/k_-^2}e_x - k_y/k_-e_y\right). \tag{9}$$

Utilizing their ray equations we can confirm the waves of the incidence ($\mathbf{k}$), the reflection ($\mathbf{k}_D$), and the transmission ($\mathbf{k}_B$) to be positively oriented, while the transmitted wave ($\mathbf{k}_C$) is negatively oriented because its group velocity $\mathbf{v}_g^C$ is antiparallel to $\mathbf{k}_C$. Momentum conservation requires that the tangential wave-vector components of $\mathbf{k}$, $\mathbf{k}_D$, $\mathbf{k}_B$, and $\mathbf{k}_C$ are equal across the interface. Energy conservation results in the incident nonpolarized electron at an oblique incident angle θ being reflected at reflection angle $-\theta$ and refracted into two polarized states with $\mathbf{k}_{B/C}$ at the refraction angles

$$\theta_{B/C} = (+/-)\arctan\left(\Theta_{+/-}/\sqrt{1-\Theta_{+/-}^2}\right), \tag{10}$$

where $\Theta_\pm = \sqrt{\varepsilon/A}/(a \pm \sqrt{\varepsilon/A})\sin\theta$. Therefore, an individual electronic beam is then bifurcated on the right side when it tunnels across the interface. The reflected and transmitted fluxes with $\mathbf{v}_g^D$ and $\mathbf{v}_g^B$ are on the opposite sides of the surface normal to that of the incident wave, while the transmitted flux with $\mathbf{v}_g^C$ is on the same side of the surface normal as that of the incidence. This signifies electronic negative refraction in the tunneling. Considering that $\mathbf{n}_A \cdot \mathbf{s}_A = +1$ and $\mathbf{n}_C \cdot \mathbf{s}_C = -1$, negative refraction corresponds to reversing the sign of ray equations when the electron crosses the interface. From the above analysis, it is shown that the transitions of an incident electronic beam to states with the same orientation characteristics as that of the incidence in the reflection and transmission exhibit normal tunneling behaviors. A transmitted state with opposite-oriented characteristics to those of the incidence displays an electronic negative refraction.

B. Negative reflection

Besides negative refraction, reversing the sign of ray equations in scattering processes at the interface of a heterostructure can also result in the occurrence of negative reflection—retroreflection. The phenomenon manifests as a reflected electron tracking the contrary path of oblique incidence. For the purpose of demonstration, we swap the left and the right sides of Fig. 1(a), i.e., $B = b\Theta(-x)$ and $C = c\Theta(-x)$, as shown in Fig. 1(b). For an incident electron with energy $\varepsilon < Aa^2$, two electron states exist, with the wave vectors ending at A' and A'' in Fig. 1(b). Their ray equations are $\mathbf{n}_{A'} \cdot \mathbf{s}_{A'} = +1$ and $\mathbf{n}_{A''} \cdot \mathbf{s}_{A''} = -1$, respectively. For an incident electron in any of these states ($\mathbf{k}_{A'}$ and $\mathbf{k}_{A''}$), there are two reflected modes $\mathbf{k}_{B'}$ and $\mathbf{k}_{C'}$, with the x components of the wave vectors smaller and larger than $k = a$.[16] These two reflected waves are in both positive- and negative-oriented states, respectively. If the ray equation of the reflected state has the same sign as that of an incident electron, the reflected mode is specular reflection. If the ray equation of the reflected state has the opposite sign to that of the incidence, the reflected mode is retroreflection. The group velocities of the $\mathbf{k}_{B'}$ reflected mode and $\mathbf{k}_{C'}$ reflected mode are

$$\mathbf{v}_g^{B'} = -2\sqrt{\varepsilon/A\hbar^2}\left(\sqrt{1-k_y^2/k_+^2}e_x - k_y/k_+e_y\right) \tag{11}$$

and

$$\mathbf{v}_g^{C'} = -2\sqrt{\varepsilon/A\hbar^2}\left(\sqrt{1-k_y^2/k_-^2}e_x + k_y/k_-e_y\right), \tag{12}$$

respectively. The angles of retroreflections are found as

$$\theta_{A'\to C'} = \pi + \arctan\left(\Theta'/\sqrt{1-\Theta'^2}\right) \tag{13}$$

for an A' electron incident at angle θ' and

$$\theta_{A''\longrightarrow B'} = \arctan\left(\Theta''/\sqrt{1-\Theta''^2}\right) \tag{14}$$

for an A'' electron incident at angle $\pi - \theta''$, where $\Theta' = [(a + \sqrt{\varepsilon/A})/(a - \sqrt{\varepsilon/A})]\sin\theta'$ and $\Theta'' = [(a - \sqrt{\varepsilon/A})/(a + \sqrt{\varepsilon/A})]\sin\theta''$.

For transmission, the ray equation of the transmitted state $\mathbf{k}_{D'}$ ($\mathbf{n}_{D'} \cdot \mathbf{s}_{D'} = +1$) has the same sign as that of incident electron $\mathbf{k}_{A'}$ but the opposite sign to that of incident electron $\mathbf{k}_{A''}$. As in the analysis in Sec. III B, the transmission for the incidence $\mathbf{k}_{A'}$ is a normal refraction, while that for incidence $\mathbf{k}_{A''}$ emerges as a negative refraction.

C. Critical incident angles

Sections III A and III B have shown that negative transport is a natural phenomenon owing to the occurrence of SOI-induced electron states whose wave vectors are in the opposite direction to their group velocities. However, the occurrence of negative refracted transmission or negative reflection is restricted by the incident angles of electronic beams. Beyond the critical angles, negative refracted transmission or negative reflection is forbidden. For example, in the case of an electron incident from a normal 2DEG to a 2DEG with SOI, two transmitted modes exist, at the wave vectors $\mathbf{k}_B$ and $\mathbf{k}_C$ on the outer circle of radius k_+ and inner circle of radius k_-, respectively. Their group velocities are given in Eqs. (8) and (9) and the refraction angles $\theta_{B/C}$ are given in Eq. (10). Because $1 + a/\sqrt{\varepsilon/A} > 1, \theta_B$ is real for all incident angles θ. However, θ_C is real only if $\theta \leqslant \arcsin(a - \sqrt{\varepsilon/A})/\sqrt{\varepsilon/A}$. Beyond $\theta_c = \arcsin(a - \sqrt{E})/\sqrt{E}$, $|k_y|$ is larger than k_- and k_x is imaginary so that the transmitted part becomes evanescent and is exponentially deceasing. Therefore, the maximum angle of incidence for the occurrence of negative refracted transmission $\mathbf{k}_C$ is θ_c.

Similarly, for reflection in heterostructures of 2DEG with and without SOI, there are two reflected modes, $\mathbf{k}_{B'}$ and $\mathbf{k}_{C'}$, when the electron is incident in the $\mathbf{k}_{A'}$ mode. The group velocities of these two reflected modes are given in Eqs. (11) and (12). The reflection angle of the specular reflection $\theta_{A'}$ is real for all possible incident angles θ. However, for reflected mode $\mathbf{k}_{C'}$, the reflection angle $\theta_{A'\to C'}$ is real only if $k_-^2 - k_+^2\sin^2\theta' \geqslant 0$. From Eq. (13) and $k_+/k_- > 1$, the reflected angle for the $\mathbf{k}_{C'}$ mode is real only if $\theta' \leqslant \arcsin[(a - \sqrt{\varepsilon/A})/(a + \sqrt{\varepsilon/A}])$. Therefore, if an incident electron is in state $\mathbf{k}_{A'}$, electron retroreflection emerges only when the incident angle θ' is smaller than the critical angle $\arcsin[(a - \sqrt{\varepsilon/A})/(a + \sqrt{\varepsilon/A})]$. The maximum critical angles of incidence relate to the appearance of evanescent modes. When the incident angle is larger than this critical angle, $k_{C',x}$ is purely imaginary and the retroreflection becomes an evanescent wave.

Different from the incident mode $\mathbf{k}_{A'}$, there is no restriction on the incident angle for the appearance of both specular reflection and retroreflection when the incident electron is in state $\mathbf{k}_{A''}$ (mode with a k vector ending at the inner edge of the equienergy surface).

IV. NEGATIVE PROPAGATING BEAMS OF ELECTRONS IN HYBRIDS OF R2DEG SYSTEMS

Besides the angular characteristics of electronic reflections and transmissions, we are also interested in the magnitudes of their fluxes. To obtain the probability current fluxes, the boundary-value problem at the interface for a concrete model has to be solved quantitatively. In the follow calculations, we consider R2DEG by taking $A = \hbar^2/2m^*$, $B = 0$, and $C = \lambda$ in Hamiltonian (5). The minimum energy of R2DEG is offset to $k_{SO} = m^*\lambda/\hbar$, as shown on the left in Fig. 1(a), where m^* is the effective mass of the electron and λ is the strength of Rashba SOI. 2DEG with a Rashba SOI is a well-studied system. A comparatively low density is possibly tuned with the gate voltage in a metal-insulator-semiconductor structure.[10–12] The proper modulations of SOI strength and electron density make the topological characteristics of the Fermi surface tunable,[13–15] abutting Rashba energy $\varepsilon_{SO} = m^*\lambda^2/2\hbar^2$, with electrons filling both spin helicity bands $\varepsilon_\pm$ or only a single helicity band ε_-. According to experiments,[10–12] we consider the case of a Fermi energy lying slightly below the energy bulging of bands. We discuss the reflected and transmitted fluxes in hybrids of N2DEG/R2DEG and R2DEG/NR2DEG [as sketched in Figs. 1(a) and 1(b), respectively]. At a low electron density, the de Broglie wavelength is large enough to envisage contacts smaller than the wavelength. The interface can be described by an infinitely narrow insulating barrier lying parallel to the y axis, $U(x) = Z\delta(x)$. Because the electronic wave packets propagate in the x-y plane, $k_{F,y}$ ($=k_F \sin\theta$) of an incident electron at an oblique angle θ can be used to parametrize solutions due to the momentum conservation in the y direction. For simplicity, we assume that the system is ballistic and the dissipation of waves can be neglected. In addition, modification of the effective masses does not change the topological characteristics of the Fermi surface. Therefore, we did not consider the modification of the effective masses in two regions. In this case, no additional complications arise and the basic physics of the phenomena under consideration is especially transparent.

A. Tunneling in a hybrid of N2DEG/R2DEG

A hybrid of N2DEG/R2DEG [Fig. 1(a)] is described by the Hamiltonian

$$H = \frac{\mathbf{p}^2}{2m^*} + \frac{1}{2\hbar}\{\lambda(x), \widehat{e}_z \cdot (\sigma \times \mathbf{p})\} + Z\delta(x), \quad (15)$$

where $\lambda(x) = \lambda\Theta(x)$. For the incident energy $\varepsilon < m^*\lambda^2/2\hbar^2$, electrons are in spin-degeneracy states in N2DEG ($x < 0$) and in spin-polarized states in R2DEG ($x > 0$). We assume that the incident electron is described by a plane wave. Its wave vector $\mathbf{k}_A$ towards the interface is at an oblique angle θ with respect to normal. The reflected wave vector $\mathbf{k}_D$ in N2DEG can be identified by the momentum conservation in the y direction because its group velocity is backwards at the interface at an angle $\pi - \theta$. The wave function in N2DEG has the form

$$\Psi_L(x,y) = \Phi_L(x)e^{ik_y y} \quad (16)$$

with

$$\Phi_L(x) = \frac{1}{\sqrt{2}}(\eta_\uparrow + \eta_\downarrow)e^{ik_x x} + (r_\uparrow\eta_\uparrow + r_\downarrow\eta_\downarrow)e^{-ik_x x}, \quad (17)$$

where $k_x = k_F\cos\theta$ and $k_y = k_F\sin\theta$, $\eta_\uparrow = (1\ 0)^{\mathcal{T}}$ and $\eta_\downarrow = (0\ 1)^{\mathcal{T}}$, and $r_\uparrow$ and $r_\downarrow$ are the reflected coefficients of the spin-up and -down components.

In R2DEG, there exist two possible transmitted modes, $\mathbf{k}_B = k_+\mathbf{n}_B$ and $\mathbf{k}_C = k_-\mathbf{n}_C$, where $k_\pm = k_{SO} \pm \sqrt{2\pi n_e}$, $\mathbf{n}_B = \cos\theta_+\widehat{e}_x + \sin\theta_+\widehat{e}_y$, and $\mathbf{n}_C = -\cos\theta_-\widehat{e}_x + \sin\theta_-\widehat{e}_y$. The refraction angles $\theta_\pm$ are given by $\theta_\pm = \arctan[\sin\theta/\sqrt{k_\pm^2/2\pi n_e - \sin^2\theta}]$. The wave function in R2DEG can be written as

$$\Psi_R(x,y) = \Phi_R(x)\, e^{ik_y y} \quad (18)$$

with

$$\Phi_R(x) = t_+\xi(\theta_+)e^{ik_{+,x}x} + t_-\xi(\theta_-)e^{-ik_{-,x}x}, \quad (19)$$

where $k_{+,x} = k_+\cos\theta_+$, $k_{-,x} = \cos\theta_-$, and $\xi(\theta_\pm) = 1/\sqrt{2}(\mp ie^{\mp i\theta_\pm}\ 1)^{\mathcal{T}}$. The coefficients t_+ and t_- are the probability amplitudes of transmitted waves with wave vectors $\mathbf{k}_B$ and $\mathbf{k}_C$. According to the analysis of ray equations in Sec. II, the transmitted mode $\mathbf{k}_B$ is normal refraction and the transmitted mode $\mathbf{k}_C$ is negative refraction.

The probability current is given by

$$\mathbf{j}(x,y) = \frac{\hbar}{m^*}\mathrm{Im}[\psi^\dagger(\nabla\psi)] + \frac{\lambda(x)}{\hbar}\psi^\dagger(\widehat{e}_z \times \sigma)\psi. \quad (20)$$

Conservation of the particle number requires that the normal components of the currents on the two sides remain in the positive x direction through the hybrid. As shown in the Appendix, the continuity conditions guarantee conservation of the probability current, i.e., $j_x^L(0) = j_x^R(0)$, where $j_x^L(x) = (\hbar/m^*)\mathrm{Im}(\Phi_L^\dagger\Phi_L')$ in the region $x < 0$ and $j_x^R(x) = (\hbar/m^*)\mathrm{Im}(\Phi_R^\dagger\Phi_R') - (\lambda/\hbar)\Phi_R^\dagger\sigma_y\Phi_R$ in the region $x > 0$. We can obtain the currents after the transport coefficients $r_\uparrow$, $r_\downarrow$, t_+, and t_- are determined. These coefficients are determined by the continuity conditions,

$$\Phi_R(0) = \Phi_L(0) \quad (21)$$

and

$$\Phi_R'(0) - \Phi_L'(0) = -\frac{2m^*}{\hbar^2}\left(Z - i\frac{\lambda}{2}\sigma_y\right)\Phi_L(0), \quad (22)$$

which is obtained by integrating the stationary form of the Schrödinger equation across an infinitesimal interval that spans the region of the δ-function potential. The normal condition for the transport coefficients $r_\uparrow$, $r_\downarrow$, t_+, and t_- can be derived,

$$|r_\uparrow|^2 + |r_\downarrow|^2 + \frac{v_g^B|t_+|^2}{v_i}\frac{\cos\theta_+}{\cos\theta} + \frac{v_g^C|t_-|^2}{v_i}\frac{\cos\theta_-}{\cos\theta} = 1, \quad (23)$$

from the conservation of the probability current at the interface, where $v_i = \hbar k_F/m^*$ and θ is the incident angle of the electronic beam.

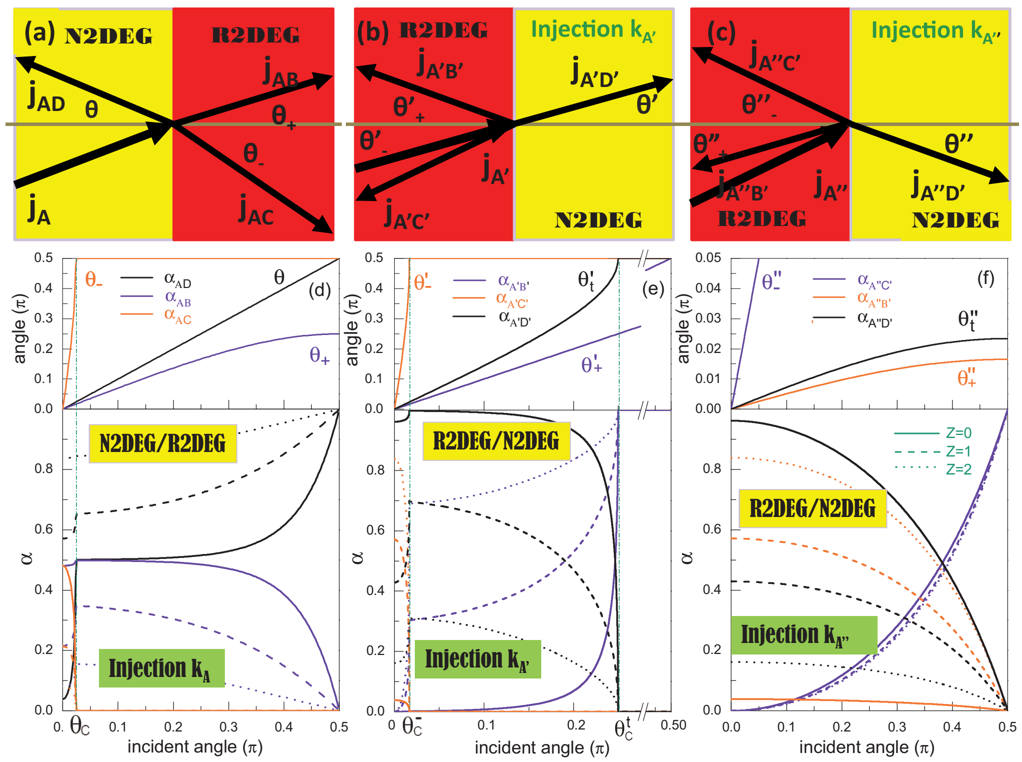

FIG. 2. (Color online) Diagram of all possible reflection and transmission processes at (a) an N2DEG/R2DEG interface and (b), (c) an R2DEG/N2DEG interface. Various transport coefficients (defined as the ratio of transport fluxes to the incident flux $\alpha = j_{\rm trans}/j_{\rm in}$) and angles in (d) for the N2DEG/R2DEG interface and (e), (f) for the R2DEG/N2DEG interface as a function of the incident angle, with the values of $Z = 0$ (solid curves), $Z = 1$ (dashed curves), $Z = 2$ (dotted curves), and $\gamma_{\rm SO} = 0.4$. (d) α_{AD} for reflection and α_{AB} for normal transmission, with α_{AC} for the negative refracted electron beam. θ_c is the critical angle of the incident electron for the appearance of a negative refracted transmission. (e), (f) $\alpha_{A'B'}$ and $\alpha_{A''C'}$ for specular reflections, $\alpha_{A'C'}$ and $\alpha_{A''B'}$ for retroreflections, and $\alpha_{A'D'}$ for normal transmission, with $\alpha_{A''D'}$ for the negative refracted transmission. θ_c^- and θ_c^t are the critical angles of the incident electron in state $\mathbf{k}_{A'}$ for the appearance of a retroreflection and transmission.

Bidirectional transmitted fluxes are given by $\mathbf{j}_{AB} = |t_+|^2\mathbf{v}_g^{(B)}$ and $\mathbf{j}_{AC} = |t_-|^2\mathbf{v}_g^{(C)}$. The flux $\mathbf{j}_{AB}$ is away from the interface inclining at an angle θ_+ to normal on the opposite side of the incidence beam $\mathbf{j}_A$. The flux $\mathbf{j}_{AC}$ is away from the interface inclining at an angle θ_- to normal on the same side of the incidence beam $\mathbf{j}_A$. Therefore, $\mathbf{j}_{AC}$ is a negative refracted flux. Defining the transport coefficients $\alpha = |\mathbf{j}_{\rm trans}|/|\mathbf{j}_{\rm in}|$, the ratio of transport fluxes to the incident flux, the angle dependence of flux magnitudes can be discussed. Taking the parameters energy of the incident electron $\varepsilon = n_e^2\varepsilon_F$, density of R2DEG $n_e \sim 1.13 \times 10^{11}/\text{cm}^{-2}$, and dimensionless SOI parameter $\gamma_{\rm SO} = 0.4$ ($\gamma_{\rm SO} = \sqrt{m^*\lambda/2\hbar^2\varepsilon_F}$), we calculate the various transport coefficients numerically. The angular dependence of the reflection and transmission coefficients (defined as the ratio of reflection and transmitted fluxes to the incident flux) are shown in Fig. 2(d). The top half of the diagram in Fig. 2(d) shows the angles of reflected and transmitted fluxes.

Figure 2(d) shows that there exists a critical angle θ_c [$=\sin^{-1}(k_-/k_F)$]. When the incident angle is larger than θ_c, negative refraction is completely forbidden. Our calculations show that negative refraction ($\alpha_{AC} = j_C/j_A$) dominates the electronic transmission at small incident angles and is strongly debilitated when the incident angle approaches θ_c. The maximum critical angles of incidence relate to the appearance of evanescent modes. When the incident angle is beyond the critical angles the transmitted modes $k_{-,x}$ will become evanescent. To obtain the solutions, we must not only match the propagating mode, but also match the evanescent mode in which $k_{-,x}$ is replaced by a purely imaginary wave vector $-i\kappa_{-,x}$. The appearance of evanescent states has been analyzed in different energy ranges in 2D systems consisting of semi-infinite regions with and without Rashba SOI.[43,44] Evanescent states for the case of a single spin-helicity band were discussed in Ref. 9 also.

B. Tunneling in a hybrid of R2DEG/N2DEG

Electronic retroreflection can be analyzed in a similar manner. We consider a hybrid of R2DEG/N2DEG as shown in Fig. 1(b). Its Hamiltonian takes the same form as Eq. (15), but $\lambda(x) = \lambda\Theta(-x)$. The electron is incident from R2DEG to N2DEG. There are two incident electron states, $\mathbf{k}_{A'} = k_+\mathbf{n}_{A'}$ and $\mathbf{k}_{A''} = k_-\mathbf{n}_{A''}$, for the incident energy $\varepsilon < m^*\lambda^2/2\hbar^2$. We first discuss the case of an incident electron in state $\mathbf{k}_{A'}$. This is a positive-oriented state and has $\mathbf{n}_{A'} \cdot \mathbf{s}_{A'} = +1$. There exist two reflected modes, $\mathbf{k}_{C'}$ and $\mathbf{k}_{B'}$, and one transmitted mode, $\mathbf{k}_{D'}$. Their ray equations are given by $\mathbf{n}_{B'} \cdot \mathbf{s}_{B'} = +1$, $\mathbf{n}_{C'} \cdot \mathbf{s}_{C'} = -1$, and $\mathbf{n}_{D'} \cdot \mathbf{s}_{D'} = +1$. The wave functions in the R2DEG and N2DEG regions are written in the form

$\Psi_{L/R}(x,y) = \Phi_{L/R}(x)e^{ik_y y}$ with

$$\Phi_L(x) = \xi(\theta_+)e^{ik_{+,x}x} + r_+\xi(\theta_+)e^{-ik_{+,x}x} + r_-\xi(\theta_-)e^{ik_{-,x}x} \tag{24}$$

and

$$\Phi_R(x) = (t_\uparrow\eta_\uparrow + t_\downarrow\eta_\downarrow)e^{ik_x x}, \tag{25}$$

where r_+ and r_- are the probability amplitudes of reflected waves with wave vectors $\mathbf{k}_{B'}$ and $\mathbf{k}_{C'}$, and $t'_\uparrow$ and $t'_\downarrow$ are the probability amplitudes of transmitted spin-up and -down components. The coefficients r_+, r_-, $t_\uparrow$, and $t_\downarrow$ can be determined by the boundary conditions $\Phi_R(0) = \Phi_L(0)$ and

$$\Phi'_R(0) - \Phi'_L(0) = -\frac{2m^*}{\hbar^2}\left(Z + i\frac{\lambda}{2}\sigma_y\right)\Phi_L(0). \tag{26}$$

Comparing the conditions, Eqs. (22) and (26), there exists a sign difference for the term $i\lambda\sigma_y/2$ on the right-hand side. The normal condition for the transport coefficients r_+, r_-, $t_\uparrow$, and $t_\downarrow$ becomes

$$|r_+|^2 + \frac{v_g^{C'}|r_-|^2}{v_g^{A'}}\frac{\cos\theta_-}{\cos\theta_+} + \left(\frac{v|t_\uparrow|^2}{v_g^{A'}} + \frac{v|t_{-\downarrow}|^2}{v_g^{A'}}\right)\frac{\cos\theta^{D'}}{\cos\theta_+} = 1. \tag{27}$$

Because the sign of the ray equation of the $\mathbf{k}_{C'}$ mode is opposite to that of $\mathbf{k}_{A'}$, while that of the $\mathbf{k}_{B'}$ mode is the same as that of $\mathbf{k}_{A'}$, the reflected flux $\mathbf{j}_{A'B'} = |r_+|^2\mathbf{v}_g^{(B')}$ is in the direction of specular reflection and the reflected flux $\mathbf{j}_{A'C'} = |r_-|^2\mathbf{v}_g^{(C')}$ is in the direction of retroreflection. The transmitted flux $\mathbf{j}_{A'D'} = (|t_\uparrow|^2 + |t_\downarrow|^2)\mathbf{v}^{(D')}$ shows a normal refracted character. The angular dependencies of the reflections $\alpha_{A'B'}$ and $\alpha_{A'C'}$ and transmission $\alpha_{A'D'}$ are illustrated in the bottom half of Fig. 2(e). It is shown that there exists a nonzero retroreflection $j_{A'C'}$ only if the incident angle $|\theta| < \theta_c^-$. Beyond the critical angle θ_c^- no propagating retroreflection appears because the wave vector of retroreflected wave $k_x^{(C')}$ becomes purely imaginary. It is shown in Fig. 2(e) that the specular reflection $j_{A'B'}$ is very small for the incident angle $|\theta| < \theta_c^-$ and the reflection is dominated by the retroreflection. As the incident angle approaches the critical angle θ_c^-, the retroreflection is strongly debilitated and the specular reflected flux increases intensely. Figure 2(e) shows a maximum critical angle θ_c^t for transmission. For the case where the densities of electrons are the same on the two sides of the interface, the Fermi surface of N2DEG is smaller than the outer circle of R2DEG. Therefore, transmission is forbidden for incident mode $\mathbf{k}^{(A')}$ if the angle of incidence exceeds the critical angle θ_c^t. To analyze the influence of the barrier potential on $\alpha_{A'B'}$, $\alpha_{A'C'}$, and $\alpha_{A'D'}$, three strengths of Z are considered. It is found that increasing the potential strength at the interface increases both the retroreflection $\mathbf{j}_{A'C'}$ and the specular reflection $\mathbf{j}_{A'B'}$.

The reflections of a $\mathbf{k}_{A''}$-incident state can be analyzed in the same way. There are also two reflected modes, $\mathbf{k}_{C'}$ and $\mathbf{k}_{B'}$, as well as one transmitted mode, $\mathbf{k}_{D'}$. Instead of (24), the wave function in the region R2DEG region is now $\Phi_L(x) = \xi(\theta_-)e^{-ik_{-,x}x} + r_+\xi(\theta_+)e^{-ik_{+,x}x} + r_-\xi(\theta_-)e^{ik_{-,x}x}$. The normal condition ensuring conservation of the probability current at the interface is given by

$$\frac{v_g^{C'}|r_+|^2}{v_g^{A''}}\frac{\cos\theta_+}{\cos\theta_-} + |r_-|^2 + \left(\frac{v|t'_\uparrow|^2}{v_g^{A''}} + \frac{v|t'_\downarrow|^2}{v_g^{A''}}\right)\frac{\cos\theta^{D'}}{\cos\theta_-} = 1. \tag{28}$$

The $\mathbf{k}_{A''}$-incident state is negatively oriented (i.e., $\mathbf{n}_{A''}\cdot\mathbf{s}_{A''} = -1$). Therefore, the reflected flux $\mathbf{j}_{A''B'} = |r'_+|^2\mathbf{v}_g^{(B')}$ is a retroreflection because the sign of its ray equation is opposite to that of the incidence. $\mathbf{j}_{A''C'} = |r'_-|^2\mathbf{v}_g^{(C')}$ is a specular reflection because its ray equation has the same sign as the incidence. For transmission, the sign of the ray equation for the transmitted mode $\mathbf{k}_{D'}$ is opposite to the incidence's of $\mathbf{k}_{A''}$. Thus, the transmitted flux $\mathbf{j}_{A''D'} = (|t'_\uparrow|^2 + |t'_\downarrow|^2)\mathbf{v}^{(D')}$ has a negatively refracted character. The angular dependencies of various fluxes are shown in the bottom half of Fig. 2(f). The angles of corresponding outgoing fluxes are illustrated in the top half of the diagram. It is found that retroreflection can occur for the full region of the incident angle. The reflection tends to be a retroreflection at a small angle of incidence but is predominated by specular reflection at a large incident angle. With an increase in the interface potential strength, the retroreflection flux $j_{A''B'}$ increases and the specular reflection $j_{A''C'}$ is suppressed.

To analyze the contributions to the tunneling current from negative processes, we can write out the total current through the R2DEG/N2DEG hybrid. Both incident processes of electrons at energy ε participate in the electronic transport through the R2DEG/N2DEG hybrid. The total conductance at zero temperature can be written in the form

$$\sigma_T = \frac{e^2}{4\pi^2\hbar}\sum_{s=\pm}\int_{-\pi/2}^{\pi/2} d\theta_s k_s(\mu)\cos\theta_s(1 - |r_s|^2) - \frac{e^2}{4\pi^2\hbar}\sum_{s=\pm}\int_{-\pi/2}^{\pi/2} d\theta_s k_s(\mu)|r_{-s}|^2\cos\theta_{-s}, \tag{29}$$

where $s = \pm 1$ stand for the spin-helicity states of incident electrons, r_s and r_{-s} are the reflection coefficients of an incident electron in the s state being reflected to the s state and $-s$ state. The terms in the second line are the angle averaged deductions from retroreflections. Figures 3(a) and 3(b) display these two deductions from the retroreflections. $\Pi_{A'} = (e^2/4\pi^2\hbar)\int_{-\pi/2}^{\pi/2} d\theta_+ k_+(\mu)|r_-|^2\cos\theta_-$ is for the $\mathbf{k}_{A'}$-incident state, while $\Pi_{A''} = (e^2/4\pi^2\hbar)\int_{-\pi/2}^{\pi/2} d\theta_- k_-(\mu)|r_+|^2\cos\theta_+$ is for the $\mathbf{k}_{A''}$-incident state. As a function of the applied voltage, it is found that the deductions from the retro-reflections diminish gradually with an increase in voltage. This is due to the deduction of the radius of the inner circle via an increasing voltage. As the consequence of momenta being decreased, retroreflected fluxes are reduced. When the voltage is increased to the value at which the energy of incident electrons reaches the energy bulging ($eV/E_{\mathrm{SO}} = 0.1875$), the inner circle shrinks to 0 [broken up by the dashed line in Figs. 3(a) and 3(b)] and the retroreflection is suppressed completely. With a further increase in voltage, the plus branch, $\varepsilon_+(k)$, begins to partake of the reflection [as shown in the right inset in Figs. 3(a) and 3(b)]. Because the ray equation for the band $\varepsilon_+(k)$ has the same sign as that of the incidence, reflection for a voltage exceeding the energy bulging emerges as a specular reflection.

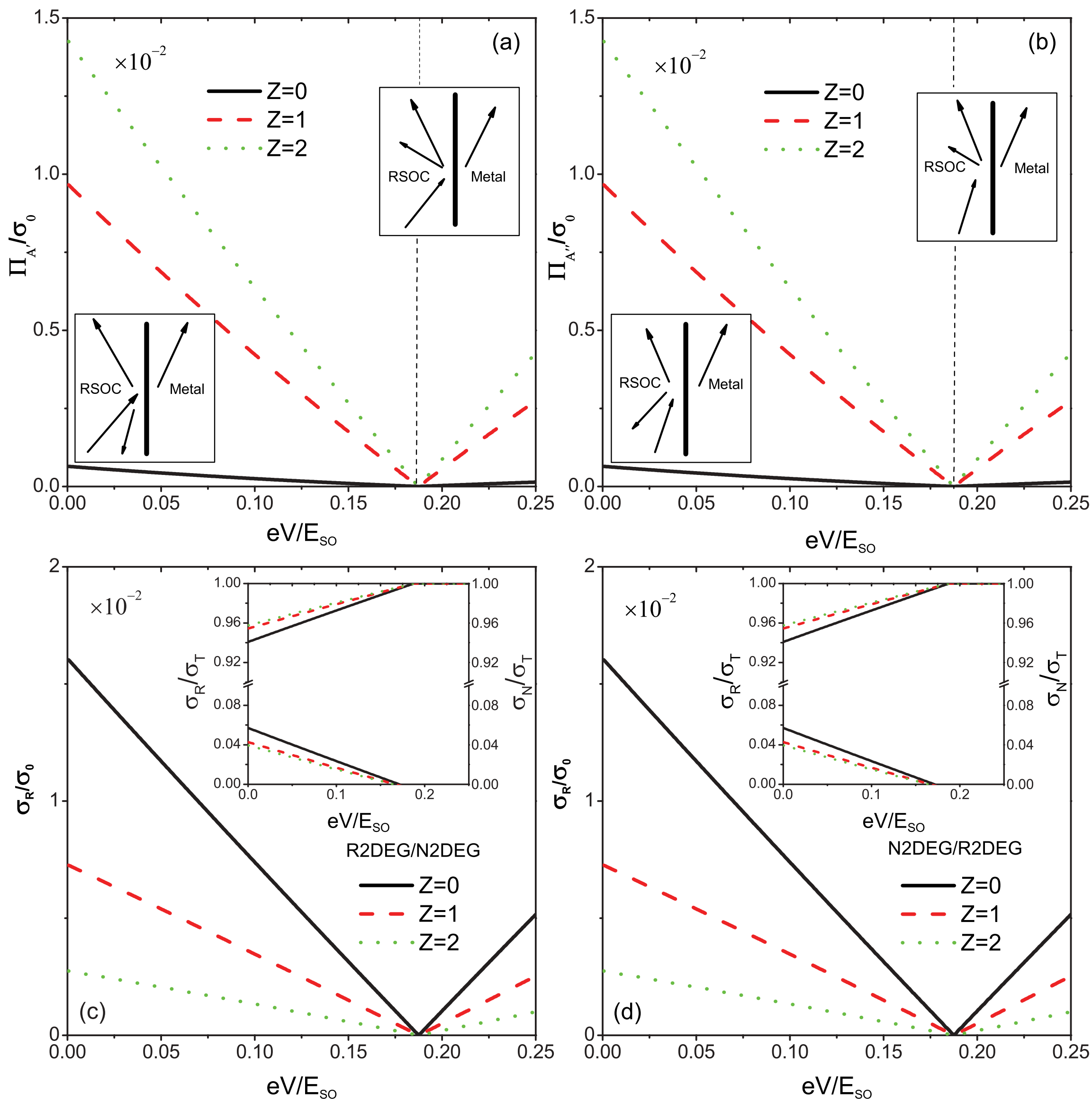

FIG. 3. (Color online) (a), (b) Deductions from retroreflections versus bias for different interface potentials: (a) for the $\mathbf{k}_{A'}$-incident state and (b) for the $\mathbf{k}_{A''}$-incident state. (c), (d) Partial conductances accrued from negative refractions versus bias: (c) for a R2DEG/N2DEG hybrid and (d) for a N2DEG/R2DEG hybrid. Insets in (c) and (d): Ratio of conductances accrued from normal transmission (upper curves) and negative transmission (lower curves) to the total conductance. The dimensionless SOI parameter $\gamma_{\rm SO} = 0.4$ ($\gamma = \sqrt{m^*\lambda/2\hbar^2 E_F}$).

In general, increasing the interface potential will increase the value of retroreflections. Figures 3(a) and 3(b) also show the phase-conjugate reflectivity[45] in the contributions from two retroreflection processes, $s \to -s$ ($s = \pm 1$).

Because the transmissions contain both normal and negative refractions, the total conductance can be written in the form $\sigma_T = \sigma_N + \sigma_R$, where σ_N is the conductance for normal transmission and σ_R is the part accrued from negative refractions. For a R2DEG/N2DEG junction, negative refraction comes from the $\mathbf{k}_{A''}$- incident state only. Utilizing the normal condition, (28), it is found that $\sigma_R = (e^2/4\pi^2\hbar)\sum_{\sigma=\uparrow,\downarrow}\int_{-\pi/2}^{\pi/2} d\theta\_k_-(\mu)(v/v_g^{(A'')})|t_\sigma|^2\cos\theta$ for the R2DEG/N2DEG hybrid. We display $\sigma_R^{\rm R2DEG/N2DEG}/\sigma_T$ via the voltage for different interface potentials in Fig. 3(c). It is found that its contribution to the total conductance is mostly concentrated around a low voltage and decreases to 0 around $eV/E_{\rm SO} = 0.1875$. Similar, the conductance from the negative refractions in N2DEG/R2DEG system can be calculated by the formula $\sigma_R = (e^2/2\pi^2\hbar)\int_{-\pi/2}^{\pi/2} d\theta k(\mu)(v_g^{(C)}/v)|t_-|^2\cos\theta_-$ for the N2DEG/R2DEG hybrid. We show $\sigma_R^{\rm N2DEG/R2DEG}/\sigma_T$ as a function of the voltage in Fig. 3(d). Figures 3(c) and 3(d) show that the conductance from negative refractions diminishes gradually with an increase in voltage. The insets in Figs. 3(c) and 3(d) show the ratio of conductances accrued from normal transmission (upper curves) to negative transmission (lower curves) to the total conductance. Especially at large interface potentials, the conductance is mainly demonstrated by normal transmission.

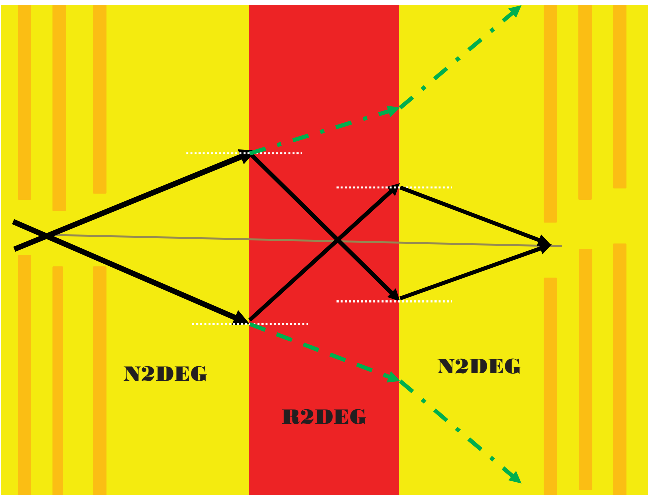

FIG. 4. (Color online) Diagram of an N2DEG/R2DEG/N2DEG sandwich structure and electron focusing.

V. ELECTRON FOCUSING

The angular distributions of negative transport fluxes reveal some interesting physics. The characteristics of existing negative transport are promising to achieve electron focusing in a suitably designed N2DEG/R2DEG/N2DEG waveguide. As depicted in Fig. 4, we utilize the transmission properties in N2DEG/R2DEG and R2DEG/N2DEG: the injected beam of nonpolarized electrons is slit into two polarized beams with opposite ray characters in R2DEG, after tunneling across the left interface of N2DEG/R2DEG. The beam with $\mathbf{n}\cdot\mathbf{s}=+1$ will disperse, but the beam with $\mathbf{n}\cdot\mathbf{s}=-1$ can be focused inside a R2DEG. These two beams in turn incident on the right interface of R2DEG/N2DEG. The beam with $\mathbf{n}\cdot\mathbf{s}=+1$ will further deflect the normal. The beam with $\mathbf{n}\cdot\mathbf{s}=-1$ will be focused again inside N2DEG. The focusing effect should manifest itself as "spot" distributions at predictable locations. For the propose of measurements, one can design two controllable output slits at the projected position of focusing in R2DEG and N2DEG (as shown in Fig. 4). An angular distribution of transmission can be observed by gating the aperture in the left N2DEG and adjusting the setting of the aperture in the right N2DEG. Since the total conductance is a macroscopic property containing contributions from all possible transport channels, it is not straightforward to separate contributions from different processes such as negative reflection and negative transmission. Although the negative transmission proposed here is an intrinsic phenomenon, it is an experimental challenge to directly quantify it with an electron beam injection via standard total conductance measurement. Therefore we suggest that the most sensitive way to experimentally identify negative transport is by fine measuring electronic focusing. In addition, utilizing the property that negative propagations have a critical angle, it is expected that the spots generated by negative transmitted beams can turn on and off with a change in the angle of the injected electronic beam.

VI. DISCUSSION AND CONCLUSIONS

In summary, we have shown the first obvious instance of realizing electronic retroreflection in electronic systems. Synthesizing the directions of transmitted fluxes $\mathbf{j}_{AC}$ and $\mathbf{j}_{A''D'}$ and reflected fluxes $\mathbf{j}_{A'C'}$, and $\mathbf{j}_{A''B'}$ in Sec. IV we demonstrate the existence of electronically negative refraction and reflection in hybrid spintronic systems with inhomogeneous SOI. We conclude that transmission or reflection emerges as negative refraction or retroreflection if the sign of the ray equation is reversed with respect to those of the incidence's in tunneling processes. From a more fundamental point of view, the physical reasons behind the characteristics of negative electronic transport come intrinsically from the occurrence of an additional electronic state with a negative group velocity, which is associated with the two-edge structure of the Fermi surface at a low electron density and strong SOI.

Utilizing the restriction on incident angles for the occurrence of negative refracted transmission and retroreflection, negative electron transport will hopefully be identified in experiments. For example, for the electronic tunneling in an R2DEG/N2DEG hybrid, we have shown that negative refracted transmission occurs only for the incident mode $\mathbf{k}_{A''}$ and not for $\mathbf{k}_{A'}$. Such a distinction between the incident modes $\mathbf{k}_{A''}$ and $\mathbf{k}_{A'}$ can be distinguished by the experimental design. Normal transmission is forbidden for the incident mode $\mathbf{k}_{A'}$ if the angle of incidence exceeds the critical angle θ_c^t; therefore, the transmission at a certain incident energy ε is negative only as soon as the incident angle is larger than θ_c^t. This property provides a means of experimental identification of negative electron refraction. We have shown that the appearance of negative transport fluxes can be used to focus a divergent electronic beam in a multilayer heterostructure consisting of semiconductors with different SOIs. Our preliminary theoretical investigation of electronic focusing has practical significance for designing new spintronic devices.

ACKNOWLEDGMENTS

We acknowledge the financial support from NBRP of China (2012CB921300) and NNSFC Grant No. 91021017, 11274013.

APPENDIX

In this Appendix we explicitly clarify the probability current conservation at the boundary. We consider an N2DEG/R2DEG heterostructure system. The Hamiltonian is given by Eq. (15) with $\lambda(x)=\lambda\Theta(x)$. Utilizing the Schrödinger equation $i\hbar\partial_t\psi = H\psi$, an equation of continuity can be derived, $\partial\rho/\partial t+\nabla\cdot\mathbf{j}=0$, where $\rho(x,y)=\psi^\dagger\psi$ is the probability density in units of particles per unit volume, and

$$\mathbf{j}(x,y)=\frac{\hbar}{m^*}\mathrm{Im}[\psi^\dagger(\nabla\psi)]+\frac{1}{\hbar}\lambda(x)\psi^\dagger(\widehat{e_z}\times\sigma)\psi \qquad \text{(A1)}$$

is the probability current in units of particles per unit area per unit time.

For a system consisting of N2DEG and R2DEG, the wave functions on the left and right sides of the interface of N2DEG/R2DEG can be written in the form $\Psi_{L/R}(x,y)=\Phi_{L/R}(x)e^{ik_y y}$ and the x components of the probability current are

$$j_x^L = \frac{\hbar}{m^*}\mathrm{Im}[\Phi_L^\dagger \Phi_L'] \tag{A2}$$

in the region $x < 0$ and

$$j_x^R = \frac{\hbar}{m^*}\mathrm{Im}[\Phi_R^\dagger \Phi_R'] - \frac{1}{\hbar}\lambda\Phi_R^\dagger\sigma_y\Phi_R \tag{A3}$$

in the region $x > 0$.

Using the boundary conditions Eqs. (21) and (22) we have

$$\mathrm{Im}[\Phi_L^\dagger \Phi_L']_{x=0} - \mathrm{Im}[\Phi_R^\dagger \Phi_R']_{x=0} = -\frac{m^*\lambda}{\hbar^2}.\Phi^\dagger\sigma_y\Phi|_{x=0}. \tag{A4}$$

This leads to $j_x^L(0) = j_x^R(0)$. It means that the boundary conditions ensure conservation of the probability current at the boundary.

In the following we derive the normal conditions for the transport coefficients which are determined from the boundary conditions. The current on the left side of the junction is found as

$$j_x^L = \frac{\hbar k_i}{m^*}[1 - (|r_\uparrow|^2 + |r_\downarrow|^2)]\cos\theta \tag{A5}$$

when we use the wave function, Eq. (17).

For the region $x > 0$ the wave function is given in Eq. (19). The current on the right side of the junction is found as

$$j_x^R = j_1 + j_2, \tag{A6}$$

where

$$j_1 = \frac{\hbar}{m^*}\sum_{s=\pm}|t_s|^2\,\xi^\dagger(\theta_s)\left(sk_{s,x} - \frac{m\lambda}{\hbar^2}\sigma_y\right)\xi(\theta_s) \tag{A7}$$

and

$$j_2 = \frac{\hbar}{m^*}\sum_{s=\pm}t_s^* t_{-s}\xi^\dagger(\theta_s)\left(s\frac{\Delta k_x}{2} - \frac{m\lambda}{\hbar^2}\sigma_y\right)\xi(\theta_{-s})e^{-isK_x x} \tag{A8}$$

with $\Delta k_x = k_{s,x} - k_{-s,x}$ and $K_x = k_{s,x} + k_{-s,x}$, where $\xi(\theta_s) = (1/\sqrt{2})(-(k_{s,y} + sik_{s,x})/k_s\ 1)^T$, $\theta_s = \tan^{-1}(k_{s,y}/k_{s,x})$, and $k_s = m\lambda/\hbar^2 + s\sqrt{m^2\lambda^2/\hbar^4 - 2mE/\hbar^2}$. Using the relations $\xi^\dagger(\theta_s)\xi(\theta_s) = 1$ and $\xi^\dagger(\theta_s)\sigma_y\xi(\theta_s) = s\cos\theta_s$, we have

$$j_1 = (v_+|t_+|^2\cos\theta_+ + v_-|t_-|^2\cos\theta_-), \tag{A9}$$

where $v_s = (\hbar/m)(k_s - m\lambda/\hbar^2)$.

The first term in the bracket of j_2 [Eq. (A8)] can be written in the form of

$$s\frac{\Delta k_x}{2}\xi^\dagger(\theta_s)\xi(\theta_{-s}) = (k_s + k_{-s})\left(\sqrt{1 - \frac{k_y^2}{k_s^2}} - \sqrt{1 - \frac{k_y^2}{k_{-s}^2}}\right) - ik_y\frac{k_s^2 - k_{-s}^2}{k_s k_{-s}}$$

due to $k_{s,y} = k_{-s,y} = k_y$. Using the relations $k_s k_{-s} = 2mE/\hbar^2$ and $k_s^2 - k_{-s}^2 = s(4m\lambda/\hbar^2)\sqrt{m^2\lambda^2/\hbar^4 - k_s k_{-s}}$, we find

$$s\frac{k_{s,x} - k_{-s,x}}{2}\xi^\dagger(\theta_s)\xi(\theta_{-s}) = i\frac{\lambda}{\hbar}\left(\frac{k_{s,y} - isk_{s,x}}{k_s} - \frac{k_{-s,y} - isk_{-s,x}}{k_{-s}}\right),$$

which cancels the second term in j_2 so that $j_2 = 0$. The probability current in the region $x > 0$ is

$$j_x^R = (v_+|t_+|^2\cos\theta_+ + v_-|t_-|^2\cos\theta_-). \tag{A10}$$

Therefore, conservation of the probability current $j_x^L = j_x^R$ leads to a normal condition among the transport coefficients $r_\uparrow$, $r_\downarrow$, t_+, and t_-,

$$|r_\uparrow|^2 + |r_\downarrow|^2 + \frac{v_+}{v_i}|t_+|^2\frac{\cos\theta_+}{\cos\theta} + \frac{v_-}{v_i}|t_-|^2\frac{\cos\theta_-}{\cos\theta} = 1, \tag{A11}$$

where $v_i = \hbar k/m^*$.

*Correspondence author: mazs@pku.edu.cn

[1] B. Datta and S. Das, Appl. Phys. Lett. **56**, 665 (1990).
[2] T. Koga, J. Nitta, H. Takayanagi, and S. Datta, Phys. Rev. Lett. **88**, 126601 (2002).
[3] S. A. Wolf, D. D. Awschalom, R. A. Buhrman, J. M. Daughton, S. von Molnr, M. L. Roukes, A. Y. Chtchelkanova, and D. M. Treger, Science **294**, 1488 (2001).
[4] I. Zǔtić, J. Fabian, and S. D. Sarma, Rev. Mod. Phys. **76**, 323 (2004).
[5] D. D. Awschalom and M. E. Flatté, Nature Phys. **3**, 153 (2007).
[6] V. M. Ramaglia, D. Bercioux, V. Cataudella, G. De Filippis, and C. A. Perroni, J. Phys.: Condens. Matter **16**, 9143 (2004).
[7] M. Khodas, A. Shekhter, and A. M. Finkel'stein, Phys. Rev. Lett. **92**, 086602 (2004).
[8] V. Teodorescu and R. Winkler, Phys. Rev. B **80**, 041311(R) (2009).
[9] V. A. Sablikov, A. A. Sukhanov, and Y. Y. Tkach, Phys. Rev. B **78**, 153302 (2008).
[10] C. R. Ast, J. Henk, A. Ernst, L. Moreschini, M. C. Falub, D. Pacilé, P. Bruno, K. Kern, and M. Grioni, Phys. Rev. Lett. **98**, 186807 (2007).
[11] C. R. Ast, D. Pacilé, L. Moreschini, M. C. Falub, M. Papagno, K. Kern, M. Grioni, J. Henk, A. Ernst, S. Ostanin, and P. Bruno, Phys. Rev. B **77**, 081407(R) (2008).
[12] L. Moreschini, A. Bendounan, H. Bentmann, M. Assig, K. Kern, F. Reinert, J. Henk, C. R. Ast, and M. Grioni, Phys. Rev. B **80**, 035438 (2009).
[13] H. Mirhosseini, A. Ernst, S. Ostanin, and J. Henk, J. Phys.: Condens. Matter **22**, 385501 (2010).
[14] P. D. C. King, R. C. Hatch, M. Bianchi, R. Ovsyannikov, C. Lupulescu, G. Landolt, B. Slomski, J. H. Dil, D. Guan, J. L. Mi, E. D. L. Rienks, J. Fink, A. Lindblad, S. Svensson, S. Bao, G. Balakrishnan, B. B. Iversen, J. Osterwalder, W. Eberhardt, F. Baumberger, and Ph. Hofmann, Phys. Rev. Lett. **107**, 096802 (2011).
[15] A. Varykhalov, D. Marchenko, M. R. Scholz, E. D. L. Rienks, T. K. Kim, G. Bihlmayer, J. Sanchez-Barriga, and O. Rader, Phys. Rev. Lett. **108**, 066804 (2012).
[16] E. B. Sonin, Phys. Rev. B **81**, 113304 (2010).
[17] E. Cappelluti, C. Grimaldi, and F. Marsiglio, Phys. Rev. Lett. **98**, 167002 (2007).

[18]E. Cappelluti, C. Grimaldi, and F. Marsiglio, Phys. Rev. B **76**, 085334 (2007).
[19]V. G. Veselago, Sov. Phys. Usp. **10**, 509 (1968).
[20]R. A. Shelby, D. R. Smith, and S. Schultz, Science **292**, 79 (2001).
[21]J. Pacheco, Jr., T. M. Grzegorczyk, B.-I. Wu, Y. Zhang, and J. A. Kong, Phys. Rev. Lett. **89**, 257401 (2002).
[22]C. G. Parazzoli, R. B. Greegor, K. Li, B. E. C. Koltenbah, and M. Tanielian, Phys. Rev. Lett. **90**, 107401 (2003).
[23]A. A. Houck, J. B. Brock, and I. L. Chuang, Phys. Rev. Lett. **90**, 137401 (2003).
[24]D. R. Smith, J. B. Pendry, and M. C. K. Wiltshire, Science **305**, 788 (2004).
[25]J. Valentine, S. Zhang, T. Zentgraf, E. Ulin-Avila, D. A. Genov, G. Bartal, and X. Zhang, Nature **455**, 376 (2008).
[26]S. Zhang, Y.-S. Park, J. Li, X. Lu, W. Zhang, and X. Zhang, Phys. Rev. Lett. **102**, 023901 (2009).
[27]J. B. Pendry, Science **306**, 1353 (2004).
[28]I. M. Frank, Pis'ma Zh. Eksp. Teor. Fiz. **28**, 482 (1978) [Sov. Phys. JETP Lett. **28**, 446 (1978)].
[29]P. V. Parimi, W. T. Lu, P. Vodo, J. Sokoloff, J. S. Derov, and S. Sridhar, Phys. Rev. Lett. **92**, 127401 (2004).
[30]G. Dolling, C. Enkrich, M. Wegener, C. M. Soukoulis, and S. Linden, Science **312**, 892 (2006).
[31]S. Foteinopoulou, E. N. Economou, and C. M. Soukoulis, Phys. Rev. Lett. **90**, 107402 (2003).
[32]G. Juzeliūnas, J. Ruseckas, A. Jacob, L. Santos, and P. Öhberg, Phys. Rev. Lett. **100**, 200405 (2008).
[33]G. Juzeliūnas, J. Ruseckas, and J. Dalibard, Phys. Rev. A **81**, 053403 (2010).
[34]V. V. Cheianov, V. Fal'ko, and B. L. Altshuler, Science **315**, 1252 (2007).
[35]X. D. Zhang, Appl. Phys. Lett. **88**, 052114 (2006).
[36]E. I. Rashba, Fiz. Tverd. Tela (Leningrad) **2**, 1224 (1960) [Sov. Phys. Solid State **2**, 1109 (1960)].
[37]Yu. A. Bychkov and E. I. Rashba, Pis'ma Zh. Eksp. Teor. Fiz. **39**, 66 (1984) [Sov. Phys. JETP Lett. **39**, 78 (1984)].
[38]G. Dresselhaus, Phys. Rev. **100**, 580 (1955).
[39]A. F. Andreev, Zh. Eksp. Teor. Fiz. **46**, 1823 (1964) [Sov. Phys. JETP **19**, 1228 (1964)].
[40]C. W. J. Beenakker, Phys. Rev. Lett. **97**, 067007 (2006).
[41]B. Lv, C. Zhang, and Z. S. Ma, Phys. Rev. Lett. **108**, 077002 (2012).
[42]I. M. Lifshitz, Zh. Eksp. Teor. Fiz. **38**, 1569 (1960) [Sov. Phys. JETP **11**, 1130 (1960)].
[43]G. Usaj and C. A. Balseiro, Europhys. Lett. **72**, 631 (2005).
[44]V. A. Sablikov and Y. Y. Tkach, Phys. Rev. B **76**, 245321 (2007).
[45]P. D. Drummond and A. T. Friberg, J. Appl. Phys. **53**, 5618 (1983).